

Magnetic Behavior of Volborthite $\text{Cu}_3\text{V}_2\text{O}_7(\text{OH})_2 \cdot 2\text{H}_2\text{O}$ Determined by Coupled Trimers Rather than Frustrated Chains

O. Janson,^{1,*} S. Furukawa,² T. Momoi,^{3,4} P. Sindzingre,⁵ J. Richter,⁶ and K. Held¹

¹*Institut für Festkörperphysik, TU Wien, Wiedner Hauptstraße 8-10, 1040 Vienna, Austria*

²*Department of Physics, University of Tokyo, 7-3-1 Hongo, Bunkyo-ku, Tokyo 113-0033, Japan*

³*Condensed Matter Theory Laboratory, RIKEN, Wako, Saitama 351-0198, Japan*

⁴*RIKEN Center for Emergent Matter Science (CEMS), Wako, Saitama 351-0198, Japan*

⁵*Laboratoire de Physique Théorique de la Matière Condensée, Université P. & M. Curie, 75252 Paris, France*

⁶*Institut für Theoretische Physik, Universität Magdeburg, D-39016 Magdeburg, Germany*

(Received 14 September 2015; revised manuscript received 24 June 2016; published 12 July 2016)

Motivated by recent experiments on volborthite single crystals showing a wide $\frac{1}{3}$ -magnetization plateau, we perform microscopic modeling by means of density functional theory (DFT) with the single-crystal structural data as a starting point. Using DFT + U , we find four leading magnetic exchanges: antiferromagnetic J and J_2 , as well as ferromagnetic J' and J_1 . Simulations of the derived spin Hamiltonian show good agreement with the experimental low-field magnetic susceptibility and high-field magnetization data. The $\frac{1}{3}$ -plateau phase pertains to polarized magnetic trimers formed by strong J bonds. An effective $J \rightarrow \infty$ model shows a tendency towards condensation of magnon bound states preceding the plateau phase.

DOI: 10.1103/PhysRevLett.117.037206

The perplexing connection between quantum magnetism and topological states of matter renewed interest in frustrated spin systems [1]. A prime example is the $S = \frac{1}{2}$ antiferromagnetic kagome Heisenberg model (KHM), whose ground state (GS) can be a gapped topological spin liquid, as suggested by large-scale density-matrix renormalization group (DMRG) simulations [2,3]. Although DMRG results were recently corroborated by nuclear magnetic resonance (NMR) measurements on herbertsmithite [4], alternative methods vouch for a gapless spin liquid [5,6] and the discussion is still not settled.

One of the remarkable properties of the KHM is the presence of field-induced gapped phases that manifest themselves as magnetization plateaus [7–9]. A key ingredient thereof is closed hexagonal loops of the kagome lattice that underlie the formation of valence-bond solid states [8]. By far the widest is the $\frac{1}{3}$ -magnetization plateau, whose structure is well described by singlets residing on closed hexagons, and polarized spins (Fig. 1, left) [7–10].

Despite the considerable progress in understanding both quantum and topological aspects of the KHM, most theoretical findings still await their experimental verification. The reason is the scarceness of material realizations: only a handful of candidate KHM materials is known to date. A prominent example is herbertsmithite, where $S = \frac{1}{2}$ spins localized on Cu^{2+} form a regular kagome lattice [12]. Other candidate materials feature exchange couplings beyond the KHM as kapellasite [13–18], haydeelite [13,17–20], francisite [21], or barlowite [22,23].

The natural mineral volborthite $\text{Cu}_3\text{V}_2\text{O}_7(\text{OH})_2 \cdot 2\text{H}_2\text{O}$ was considered a promising KHM material [24,25], until it was noticed that the local environment of two

crystallographically distinct Cu sites hints at different magnetically active orbitals [26]. Density functional theory (DFT) calculations show that this has dramatic implications for the spin physics, giving rise to coupled frustrated chains (CFCs) with ferromagnetic (FM) nearest-neighbor and antiferromagnetic (AF) second-neighbor exchanges, and interstitial spins that are AF coupled to the two neighboring chains [11]. However, detailed structural studies reveal that below ~ 300 K all Cu atoms have the $d_{x^2-y^2}$ as the magnetically active orbital [27], questioning the applicability of the CFC model for volborthite. Furthermore, the CFC model features the $\frac{1}{3}$ -magnetization plateau with a semiclassical “up-up-down” structure (Fig. 1, middle), which was never observed in powder samples [28,29]. Recent magnetization measurements on single crystals overturned the experimental situation: a broad $\frac{1}{3}$ -magnetization plateau sets in at $H_{c1} \approx 26$ T and continues up to at least 74 T [30].

Puzzled by the remarkable difference between the single-crystal and powder data, we adopt the structural model

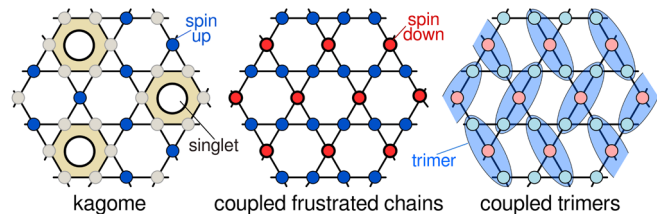


FIG. 1. The structure of the $\frac{1}{3}$ -magnetization plateau in the kagome model (KHM), coupled frustrated chains (CFC) model from Ref. [11], and the J - J' - J_1 - J_2 model.

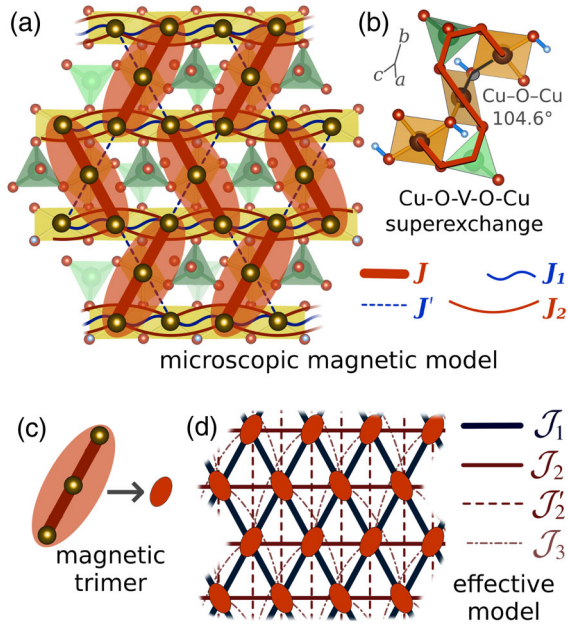


FIG. 2. (a) Microscopic magnetic model of volborthite featuring four relevant exchange couplings: antiferromagnetic J (thick bars) and J_2 (solid curved lines), as well as ferromagnetic J' (dashed lines) and J_1 (wiggly lines). Magnetic trimers formed by J exchanges are highlighted (shaded ovals). Magnetic Cu atoms are shown as large spheres within CuO_4 squares, nonmagnetic V atoms are middle-sized spheres within VO_4 tetrahedra. (b) The Cu-O-V-O-Cu superexchange paths in the magnetic trimer. (c) Magnetic trimers form a basis for (d) the effective model with ferromagnetic \mathcal{J}_1 , as well as antiferromagnetic \mathcal{J}_2 , \mathcal{J}'_2 , and \mathcal{J}_3 .

from Ref. [30] and perform DFT and DFT + U calculations. We find a microscopic model which is even more involved than CFC: besides sizable J_1 and J_2 forming frustrated spin chains, the coupling between the chain and the interstitial Cu atoms is now facilitated by two *inequivalent* exchanges, a sizable AF J and a much weaker FM J' . Because of the dominance of J , the magnetic planes break up into magnetic trimers (Fig. 2). By using exact diagonalization (ED) of the spin Hamiltonian, we demonstrate that this model agrees with the experimental magnetization data and explains the nature of the plateau phase

(Fig. 1, right). Further insight into the low-field and low-temperature properties of volborthite is provided by analyzing effective models of pseudospin- $\frac{1}{2}$ moments T living on trimers. Thus, a model based on effective exchanges \mathcal{J}_1 , \mathcal{J}_2 , and \mathcal{J}'_2 supports the presence of a bond nematic phase due to the condensation of two-magnon bound states. Finally, we conjecture that powder samples of volborthite suffer from disorder effects pertaining to the stretching distortion of Cu octahedra.

We start our analysis with a careful consideration of the crystal structure. Volborthite features a layered structure, with kagomelike planes that are well separated by water molecules and nonmagnetic V_2O_7 groups. Magnetic Cu^{2+} atoms within the planes occupy two different sites: Cu(2) with four short Cu-O bonds forms edge-sharing chains, and interstitial Cu(1) located in between the chains. Different structural models in the literature suggest either squeezed [31] or stretched [32] $\text{Cu}(1)\text{O}_6$ octahedra. The DFT study of Ref. [11] employed a structure with a squeezed Cu(1) octahedron. Although such a configuration can be realized at high temperatures [27], $\text{Cu}(1)\text{O}_6$ octahedra are actually stretched in the temperature range relevant to magnetism [27,30]. The respective structural model was never studied with DFT; hence, we fill this gap with the present study.

For DFT calculations [33], we use the generalized gradient approximation (GGA) [44] as implemented in the full-potential code FPLO9.07-41 [45]. We start with a critical examination of all structural models proposed so far, by optimizing the H coordinates and comparing the total energies. In this way, we find that the single crystal structure of Ref. [30] has the lowest total energy [33]. All further calculations are done for this structural data set.

To evaluate the magnetic couplings, we project the relevant GGA bands onto Cu-centered Wannier functions [33]. The leading transfer integrals t (> 50 meV) of the resulting one-orbital ($d_{x^2-y^2}$) model are provided in Table I. Their squared values are proportional to the AF superexchange, which is usually the leading contribution to the magnetism. However, such a one-orbital model fully neglects FM contributions that are particularly strong for short-range couplings ($d_{\text{Cu}\dots\text{Cu}} \lesssim 3$ Å). Hence, to evaluate the exchange integrals that comprise AF and FM

TABLE I. Direct Cu...Cu distances $d_{\text{Cu}\dots\text{Cu}}$ (in Å), transfer integrals t (in meV) and exchange integrals J (in K). GGA + U results are provided for three different values of the on-site Coulomb repulsion U_d . The two numbers in each entry pertain to the two structurally inequivalent layers; this minor layer dependence is ignored in the subsequent analysis.

| | $d_{\text{Cu}\dots\text{Cu}}$ | t | J (GGA + U) | | |
|-------|-------------------------------|------------|------------------|----------|----------|
| | | | $U_d = 8.5$ eV | 9.5 eV | 10.5 eV |
| J | 3.053/3.058 | -191/ -194 | 193/205 | 156/167 | 127/136 |
| J' | 3.016/3.020 | -80/ -84 | -29/ -22 | -30/ -25 | -32/ -26 |
| J_1 | 2.922/2.923 | -98/ -100 | -65/ -65 | -76/ -74 | -77/ -76 |
| J_2 | 5.842/5.842 | 64/64 | 32/31 | 26/22 | 22/21 |

contributions, we perform DFT + U calculations for magnetic supercells and map the total energies onto a Heisenberg model. These results are summarized in Table I.

Prior to discussing the magnetic model, we should note that the structural model of Ref. [30] implies the presence of two similar, albeit symmetrically inequivalent magnetic layers, with slightly different Cu...Cu distances. Since the respective transfer (t) and exchange (J) integrals for both layers are nearly identical (Table I), we can approximately assume that all layers are equal and halve the number of independent terms in the model.

The resulting four exchanges, J , J' , J_1 , and J_2 , form the 2D microscopic magnetic model depicted in Fig. 2. This model is topologically equivalent to the CFC model: it consists of chains with first- (J_1) and second-neighbor (J_2) couplings and the interstitial Cu atoms coupled to two neighboring chains. However, the exchange between the interstitial spins and the chains is realized by two different terms: a dominant AF J and much weaker FM J' . This contrasts with the CFC model, where both exchanges are equivalent ($J = J'$).

From the structural considerations, the difference between J and J' may seem bewildering, as Cu...Cu distances (Table I) and Cu-O-Cu angles (104.6° versus 102.4°) are very similar. Indeed, for the usual Cu-O-Cu path, the superexchange would be only marginally different for J and J' . The difference originates from the long-range Cu-O-V-O-Cu path [Fig. 2(b)] which provides an additional contribution to J , but not J' , since the latter lacks a bridging VO_4 tetrahedron. It is known that long-range superexchange involving empty V d states can facilitate a sizable magnetic exchange of up to 300 K [46]. Hence, it is the long-range Cu-O-V-O-Cu superexchange that renders J much stronger than J' .

A distinct hierarchy of the exchanges $J > |J_1| > J_2, J'$ leads to a simple and instructive physical picture. The dominant exchange J couples spins into trimers that tile the magnetic layers. Each trimer is connected to its four nearest neighbors by FM J' and J_1 , and to its two second neighbors by AF J_2 (Fig. 2). In contrast to the CFC model, where frustration is driven exclusively by J_2 , the coupled trimer model has an additional source of frustration: triangular loops formed by J , J' , and J_1 . Together with J_2 , they act against long-range magnetic ordering.

DFT + U -based numerical estimates for the leading exchange couplings allow us to address the experimental data. To simulate the temperature dependence of the magnetic susceptibility χ , ED of the spin Hamiltonian is performed on lattices of $N = 24$ spins, using the approximate ratios of the exchange integrals $J:J':J_1:J_2 = 1:-0.2:-0.5:0.2$ (Table I). The simulated curves are fitted to the experiment by treating the overall energy scale J , the Landé factor g , and the temperature-independent contribution χ_0 as free parameters. In this way, we obtain a good fit down to 35 K with $J = 252$ K, $g = 2.151$, and

$\chi_0 = 1.06 \times 10^{-4}$ emu/[mol Cu] (Fig. 3). ED even reproduces the broad maximum at 18 K, which stems from short-range antiferromagnetic correlations. Deviations at lower temperatures are finite-size effects.

After establishing good agreement with the $\chi(T)$ data, we employ a larger lattice of $N = 36$ spins and calculate the GS magnetization curve, which shows a wide $\frac{1}{3}$ -magnetization plateau between the critical fields H_{c1} and H_{c2} (Fig. 3, bottom left). Scaling with J and g from the $\chi(T)$ fit, without any adjustable parameters, yields $H_{c1} = 22$ T in agreement with the experimental $H_{c1} = 26$ T. In the plateau phase, first- and second-neighbor spin correlations within each trimer amount to $\langle \mathbf{S}_0 \cdot \mathbf{S}_1 \rangle \equiv \langle \mathbf{S}_1 \cdot \mathbf{S}_2 \rangle = -0.4938$ and $\langle \mathbf{S}_0 \cdot \mathbf{S}_2 \rangle = 0.2470$, very close to the isolated trimer result ($-\frac{1}{2}$ and $\frac{1}{4}$, respectively [33]). Hence, the $\frac{1}{3}$ -plateau phase can be approximated by a product of polarized spin trimers formed by strong J bonds (Fig. 1, right), and thus is very different from the plateau phases of the KHM (Fig. 1, left) and the CFC model (Fig. 1, middle). The plateau stretches up to a remarkably high $H_{c2} \approx 225$ T, at which the spin trimers break up, allowing the magnetization to triple.

ED-simulated spin correlations indicate that the simplest effective model—the isolated trimer model—already captures the nature of this plateau phase. On general grounds, we can expect the isolated trimer model to be valid only at high temperatures. However, it provides a surprisingly good fit for magnetic susceptibility down to 60 K

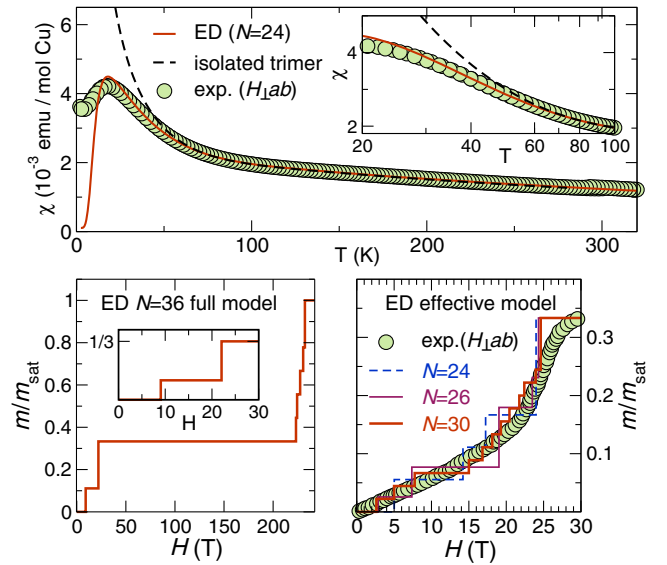


FIG. 3. Top: Magnetic susceptibility of the microscopic spin Hamiltonian calculated by ED on a $N = 24$ site lattice compared to experiment (Ref. [47]) and an isolated trimer model. Bottom left: GS magnetization curve simulated on a lattice of $N = 36$ spins for the same model. Insets are magnifications of the respective data. Bottom right: GS magnetization of the full effective model [33] with $N = 24, 26,$ and 30 pseudospins compared to experiment (Ref. [30]).

(Fig. 3, top), i.e., at a much weaker energy scale than the leading exchange $J \approx 250$ K (Fig. 3). This motivates us to treat the intertrimer couplings perturbatively and derive a more elaborate effective model valid at low temperatures and in low fields ($T, g\mu_B H/k_B \ll J$).

To this end, we adopt the lowest-energy doublet of each trimer at $H = 0$ as the basis for a pseudospin- $\frac{1}{2}$ operator \mathbf{T}_i . The $\frac{1}{3}$ -plateau phase corresponds to the full polarization of pseudospin- $\frac{1}{2}$ moments ($m_{\text{sat}}^{\text{eff}} = m_{\text{sat}}/3$). Degenerate perturbation theory to second order in the intertrimer couplings yields an effective Heisenberg model on a triangular lattice with spatially anisotropic nearest-neighbor couplings $\mathcal{J}_1 = -34.9$ K and $\mathcal{J}_2 = 36.5$ K and much weaker longer-range couplings such as $\mathcal{J}'_2 = 6.8$ K and $\mathcal{J}_3 = 4.6$ K shown in Fig. 2(d) [33]. The competition between FM \mathcal{J}_1 and AF \mathcal{J}_2 underlies the frustrated nature of the effective model. Larger finite lattices available to ED of the effective model allow us to amend the critical field H_{c1} estimate compared to the full microscopic model (Fig. 3, bottom left) and reproduce a pronounced change in the $M(H)$ slope (Fig. 3, bottom right), which agrees with the experimental kink at ~ 22 T [30].

Effective models provide important insights into the nature of field-induced states. Recent NMR experiments on single crystals revealed the emergence of the incommensurate collinear spin-density-wave (SDW) phase “II” ($H < 23$ T) and the “N” phase preceding the plateau ($23 \text{ T} < H < 26 \text{ T}$) [30]. We first address the nature of the latter phase, by treating the fully polarized pseudospin state (the $1/3$ -plateau state of volborthite) as the vacuum and analyzing the magnon instabilities to it.

To this end, we resort to a model with three leading effective couplings \mathcal{J}_1 , \mathcal{J}_2 , and \mathcal{J}'_2 . This model is equivalent to the frustrated FM square lattice model, where a bond nematic order emerges owing to condensation of two-magnon bound states (bimagnons) for $\mathcal{J}_2 = \mathcal{J}'_2 \gtrsim 0.4|\mathcal{J}_1|$ [48]. Here we take the approximate ratio $|\mathcal{J}_2/\mathcal{J}_1| = 1$ of the perturbative estimates, and study the influence of \mathcal{J}'_2 on the ground state. We find that the bond nematic order is robust for $|\mathcal{J}'_2/\mathcal{J}_1| \gtrsim 0.3$ [33], as signaled by the occurrence of bimagnon condensation at $H_{c1}^{(2)}$, at which the plateau state is already destabilized, but before single-magnon condensation sets in at $H_{c1}^{(1)}$ [Fig. 4(a)]. The bond nematic phase shows no long-range magnetic order besides the field-induced moment, but it is characterized by a bond order with an alternating sign of directors $D_{ij} \equiv \langle T_i^x T_j^x - T_i^y T_j^y \rangle$ residing on \mathcal{J}_1 bonds [Fig. 4(b)] [49]. This phase is a viable candidate for the experimentally observed “N” phase, whose NMR spectra are not explained by simple magnetic orders [30].

While bimagnons are stable in a wide region of the \mathcal{J}_1 - \mathcal{J}_2 - \mathcal{J}'_2 model, longer-range effective couplings such as \mathcal{J}_3 tend to destabilize bimagnons. However, a slight tuning of the microscopic model (e.g., increasing of $|J'|$) can counteract this effect, thereby recovering the nematic phase

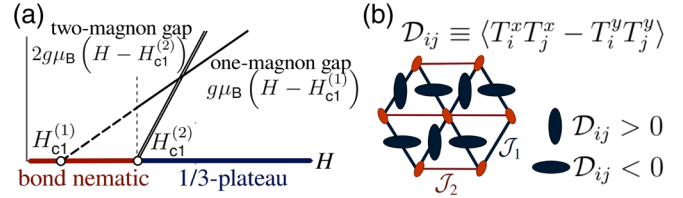


FIG. 4. (a) The behavior of one- and two-magnon gaps in the $\frac{1}{3}$ -plateau phase, which gives rise to a bond nematic phase. (b) Schematic picture of the bond nematic phase in the effective model. Orientation of dark ellipses represents the sign of directors D_{ij} on \mathcal{J}_1 bonds [49].

[33]. Long-range effective couplings are also sensitive to weak long-range exchanges neglected in the full microscopic model. In the absence of experimental estimates for these small exchanges, the \mathcal{J}_1 - \mathcal{J}_2 - \mathcal{J}'_2 effective model is an adequate approximation, which allows us to study the nature of the field-induced phases in volborthite.

Below 23 T, NMR spectra indicate the onset of an incommensurate collinear phase II [30]. Unfortunately, incommensurate spin correlations produce irregular finite-size effects that impede an ED simulation. Yet, on a qualitative level, further truncation of the model to the effective couplings \mathcal{J}_1 and \mathcal{J}_2 leads to an anisotropic triangular model, for which a field-theory analysis predicts the SDW order for $m \lesssim \frac{2}{3} m_{\text{sat}}^{\text{eff}} = \frac{2}{9} m_{\text{sat}}$ [50].

Next, we go a step beyond the Heisenberg model and consider antisymmetric Dzyaloshinskii-Moriya (DM) components for the leading couplings J and J_1 . By performing noncollinear DFT + U calculations with VASP [51], we obtain $|D_1|/J_1 \approx 0.12$ with \vec{D}_1 nearly orthogonal to the frustrated chains. DM vectors \vec{D} within the trimers are nearly orthogonal to the respective interatomic vectors and amount to $|D|/J \approx 0.09$ [33]. We analyzed the influence of D for isolated dimers with ED and found a minute change in spin correlations in the plateau state, which amounts to 2% at most. However, these DM interactions are the leading anisotropy at low fields, and can give rise to the two consecutive transitions to the incommensurate phase I ($T < 1$ K, $H < 4$ T) [27].

Finally, we address the intriguing question why the $\frac{1}{3}$ plateau has not been observed in powder samples. We remind the reader that the trimers are underlain by the stretching distortion of $\text{Cu}(1)\text{O}_6$ octahedra, which selects two out of four neighboring VO_4 octahedra for the J superexchange pathway [Fig. 2(b)]. In single crystals, the distortion axes are fixed, and the trimers form an ordered parquetlike pattern. Powder samples, on the other hand, are more prone to a random choice of the distortion axis. A single defect of this type permutes J and J' , ruining the trimer picture locally. This tentative scenario explains the absence of a plateau and the strong dependence on the sample quality in the powder magnetization data.

In summary, the stretching distortion of the magnetic $\text{Cu}(1)\text{O}_6$ octahedra in volborthite leads to the model of

coupled trimers, very different from the anisotropic kagome and coupled frustrated chain models discussed in earlier studies. Based on DFT calculations and ED simulations, we conclude that (i) the microscopic magnetic model of volborthite contains four exchanges with a ratio $J:J':J_1:J_2 = 1: -0.2: -0.5:0.2$ and $J = 252$ K, (ii) the $\frac{1}{3}$ -magnetization plateau can be understood as a product of nearly independent polarized trimers, and (iii) the effective $\mathcal{J}_1\text{-}\mathcal{J}_2\text{-}\mathcal{J}'_2$ model shows indications for a bond nematic phase which precedes the onset of the plateau.

We thank H. Ishikawa, M. Yoshida, T. Yamashita, Z. Hiroi, H. Rosner, and N. Shannon for fruitful discussions. O. J. and K. H. were supported by the European Research Council under the European Unions Seventh Framework Program FP7/ERC through Grant Agreement No. 306447. S. F. and T. M. were supported by JSPS KAKENHI Grants No. 25800225 and No. 23540397, respectively.

Note added.—A recent NMR study [52] supports our bond nematic phase scenario below the $\frac{1}{3}$ plateau.

*olegjanson@gmail.com

- [1] L. Balents, *Nature (London)* **464**, 199 (2010).
- [2] S. Yan, D. A. Huse, and S. R. White, *Science* **332**, 1173 (2011).
- [3] S. Depenbrock, I. P. McCulloch, and U. Schollwöck, *Phys. Rev. Lett.* **109**, 067201 (2012).
- [4] M. Fu, T. Imai, T.-H. Han, and Y. S. Lee, *Science* **350**, 655 (2015).
- [5] Y. Iqbal, F. Becca, and D. Poilblanc, *Phys. Rev. B* **84**, 020407 (2011).
- [6] Y. Iqbal, D. Poilblanc, and F. Becca, *Phys. Rev. B* **89**, 020407 (2014).
- [7] S. Nishimoto, N. Shibata, and C. Hotta, *Nat. Commun.* **4**, 2287 (2013).
- [8] S. Capponi, O. Derzhko, A. Honecker, A. M. Läuchli, and J. Richter, *Phys. Rev. B* **88**, 144416 (2013).
- [9] J. Schulenburg, A. Honecker, J. Schnack, J. Richter, and H.-J. Schmidt, *Phys. Rev. Lett.* **88**, 167207 (2002).
- [10] D. C. Cabra, M. D. Grynberg, P. C. W. Holdsworth, A. Honecker, P. Pujol, J. Richter, D. Schmalfuß, and J. Schulenburg, *Phys. Rev. B* **71**, 144420 (2005).
- [11] O. Janson, J. Richter, P. Sindzingre, and H. Rosner, *Phys. Rev. B* **82**, 104434 (2010).
- [12] J. S. Helton, K. Matan, M. P. Shores, E. A. Nytko, B. M. Bartlett, Y. Yoshida, Y. Takano, A. Suslov, Y. Qiu, J.-H. Chung, D. G. Nocera, and Y. S. Lee, *Phys. Rev. Lett.* **98**, 107204 (2007).
- [13] O. Janson, J. Richter, and H. Rosner, *Phys. Rev. Lett.* **101**, 106403 (2008).
- [14] R. H. Colman, C. Ritter, and A. S. Wills, *Chem. Mater.* **20**, 6897 (2008).
- [15] B. Fåk, E. Kermarrec, L. Messio, B. Bernu, C. Lhuillier, F. Bert, P. Mendels, B. Koteswararao, F. Bouquet, J. Ollivier, A. D. Hillier, A. Amato, R. H. Colman, and A. S. Wills, *Phys. Rev. Lett.* **109**, 037208 (2012).
- [16] H. O. Jeschke, F. Salvat-Pujol, and R. Valentí, *Phys. Rev. B* **88**, 075106 (2013).
- [17] Y. Iqbal, H. O. Jeschke, J. Reuther, R. Valentí, I. I. Mazin, M. Greiter, and R. Thomale, *Phys. Rev. B* **92**, 220404 (2015).
- [18] S. Bieri, L. Messio, B. Bernu, and C. Lhuillier, *Phys. Rev. B* **92**, 060407 (2015).
- [19] R. H. Colman, A. Sinclair, and A. S. Wills, *Chem. Mater.* **22**, 5774 (2010).
- [20] D. Boldrin, B. Fåk, M. Enderle, S. Bieri, J. Ollivier, S. Rols, P. Manuel, and A. S. Wills, *Phys. Rev. B* **91**, 220408 (2015).
- [21] I. Rousochatzakis, J. Richter, R. Zinke, and A. A. Tsirlin, *Phys. Rev. B* **91**, 024416 (2015).
- [22] T.-H. Han, J. Singleton, and J. A. Schlueter, *Phys. Rev. Lett.* **113**, 227203 (2014).
- [23] H. O. Jeschke, F. Salvat-Pujol, E. Gati, N. H. Hoang, B. Wolf, M. Lang, J. A. Schlueter, and R. Valentí, *Phys. Rev. B* **92**, 094417 (2015).
- [24] Z. Hiroi, M. Hanawa, N. Kobayashi, M. Nohara, H. Takagi, Y. Kato, and M. Takigawa, *J. Phys. Soc. Jpn.* **70**, 3377 (2001).
- [25] F. Bert, D. Bono, P. Mendels, F. Ladieu, F. Duc, J.-C. Trombe, and P. Millet, *Phys. Rev. Lett.* **95**, 087203 (2005).
- [26] Y. Okamoto, H. Yoshida, and Z. Hiroi, *J. Phys. Soc. Jpn.* **78**, 033701 (2009).
- [27] H. Yoshida, J. Yamaura, M. Isobe, Y. Okamoto, G. J. Nilsen, and Z. Hiroi, *Nat. Commun.* **3**, 860 (2012).
- [28] H. Yoshida, Y. Okamoto, T. Tayama, T. Sakakibara, M. Tokunaga, A. Matsuo, Y. Narumi, K. Kindo, M. Yoshida, M. Takigawa, and Z. Hiroi, *J. Phys. Soc. Jpn.* **78**, 043704 (2009).
- [29] Y. Okamoto, M. Tokunaga, H. Yoshida, A. Matsuo, K. Kindo, and Z. Hiroi, *Phys. Rev. B* **83**, 180407 (2011).
- [30] H. Ishikawa, M. Yoshida, K. Nawa, M. Jeong, S. Krämer, M. Horvatić, C. Berthier, M. Takigawa, M. Akaki, A. Miyake, M. Tokunaga, K. Kindo, J. Yamaura, Y. Okamoto, and Z. Hiroi, *Phys. Rev. Lett.* **114**, 227202 (2015).
- [31] R. Basso, A. Palenzona, and L. Zefiro, *N. Jb. Miner. Mh.* **9**, 385 (1988); M. A. Lafontaine, A. Le Bail, and G. Férey, *J. Solid State Chem.* **85**, 220 (1990).
- [32] A. Kashaev, I. Rozhdestvenskaya, I. Bannova, A. Sapozhnikov, and O. Glebova, *J. Struct. Chem.* **49**, 708 (2008); H. Ishikawa, J. Yamaura, Y. Okamoto, H. Yoshida, G. J. Nilsen, and Z. Hiroi, *Acta Crystallogr.* **C68**, i41 (2012).
- [33] See Supplemental Material at <http://link.aps.org/supplemental/10.1103/PhysRevLett.117.037206> for details of DFT calculations, the evaluation of DM vectors, crystal structures, Wannier functions (WF) projections for a two-orbital model, the derivation of effective Hamiltonians, and the details of their one- and two-magnon spectra. The Supplemental Material includes Refs. [34–43].
- [34] J. P. Perdew and Y. Wang, *Phys. Rev. B* **45**, 13244 (1992).
- [35] H. Xiang, C. Lee, H.-J. Koo, X. Gong, and M.-H. Whangbo, *Dalton Trans.* **42**, 823 (2013).
- [36] F. Mila and K. P. Schmidt, in *Introduction to Frustrated Magnetism*, edited by C. Lacroix, P. Mendels, and F. Mila (Springer-Verlag, Berlin, Heidelberg, 2011), pp. 537–562.
- [37] K. Totsuka, *Phys. Rev. B* **57**, 3454 (1998).

- [38] F. Mila, *Eur. Phys. J. B* **6**, 201 (1998).
- [39] T. Tonegawa, K. Okamoto, T. Hikihara, Y. Takahashi, and M. Kaburagi, *J. Phys. Soc. Jpn.* **69**(Suppl. A), 332 (2000).
- [40] A. Honecker and A. Läuchli, *Phys. Rev. B* **63**, 174407 (2001).
- [41] L. Kecke, T. Momoi, and A. Furusaki, *Phys. Rev. B* **76**, 060407 (2007).
- [42] J. M. Luttinger and L. Tisza, *Phys. Rev.* **70**, 954 (1946).
- [43] H. Nishimori, http://www.stat.phys.titech.ac.jp/~nishimori/titpack2_new/index-e.html.
- [44] J. P. Perdew, K. Burke, and M. Ernzerhof, *Phys. Rev. Lett.* **77**, 3865 (1996).
- [45] K. Koepnik and H. Eschrig, *Phys. Rev. B* **59**, 1743 (1999).
- [46] A. Möller, M. Schmitt, W. Schnelle, T. Förster, and H. Rosner, *Phys. Rev. B* **80**, 125106 (2009).
- [47] H. Ishikawa (private communication).
- [48] N. Shannon, T. Momoi, and P. Sindzingre, *Phys. Rev. Lett.* **96**, 027213 (2006).
- [49] In a magnetic field, the transverse component of a bond nematic order can be decomposed into the $x^2 - y^2$ component given by $D_{ij} \propto \cos 2\theta$ and the xy component $\propto \sin 2\theta$, where θ is the rotation around the z axis [48]. Symmetry breaking will pick one specific θ , which we set to $\theta = 0$ ($\theta = (\pi/2)$ follows on the neighboring sites). Hence the xy component vanishes, and D_{ij} acquires alternating signs on the neighboring bonds (Fig. 4, right).
- [50] O. A. Starykh, H. Katsura, and L. Balents, *Phys. Rev. B* **82**, 014421 (2010).
- [51] G. Kresse and J. Furthmüller, *Phys. Rev. B* **54**, 11169 (1996); *Comput. Mater. Sci.* **6**, 15 (1996).
- [52] M. Yoshida, K. Nawa, H. Ishikawa, M. Takigawa, M. Jeong, S. Kramer, M. Horvatić, C. Berthier, K. Matsui, T. Goto, S. Kimura, T. Sasaki, J. Yamaura, H. Yoshida, Y. Okamoto, and Z. Hiroi, [arXiv:1602.04028](https://arxiv.org/abs/1602.04028).